RSC Advances

PAPER

View Article Online
View Journal | View Issue

Cite this: *RSC Adv.*, 2015, **5**, 99658

Enhancing the charge separation and migration efficiency of Bi_2WO_6 by hybridizing the P3HT conducting polymer

Tingting Zheng, Jiayue Xu,* Zhijie Zhang* and Haibo Zeng

Received 8th September 2015
Accepted 12th November 2015

DOI: 10.1039/c5ra18301d

www.rsc.org/advances

In order to improve the charge separation and migration efficiency, a conducting polymer, poly(3-hexylthiophene) (P3HT), was introduced into a Bi_2WO_6 photocatalyst. The hall mobility of the P3HT/Bi_2WO_6 composite and bare Bi_2WO_6 were 4.7197 $\times$ 10^2 cm^2 V^{-1} s^{-1} and 3.0159 $\times$ 10^2 cm^2 V^{-1} s^{-1}, respectively, indicating the high charge transfer ability of the P3HT/Bi_2WO_6 composite. The photodegradation of a model pollutant, rhodamine B (RhB) under simulated solar light irradiation, demonstrated that the P3HT/Bi_2WO_6 composite showed more enhanced photocatalytic activity than bare Bi_2WO_6. The excellent photocatalytic performance of the P3HT/Bi_2WO_6 composite could be ascribed to the internal electric field formed between n-type Bi_2WO_6 and p-type P3HT, which facilitates the separation of photo-generated electron–hole pairs, as well as the high charge carrier mobility of P3HT, which can transport the photo-generated holes to the surface of the semiconductor quickly to participate in the oxidation of pollutants.

1. Introduction

With the increasing global environmental problems, the potential application of photocatalysis in environmental purification has aroused widespread concern in the past few decades.[1,2] In principle, heterogeneous photocatalysis involves the generation, separation and migration of photo-induced charge carriers, which undergo redox reactions with the adsorbed substrates on the surface of the semiconductor.[3,4] The desired photocatalysts are expected to promote the charge transfer process while suppressing the recombination process. Unfortunately, due to the fast recombination rate of photo-induced electron–hole pairs, the photocatalytic systems developed thus far have been restricted by their low efficiency.[5,6] Therefore, in order to expand the application of photocatalysis, it is important to facilitate the charge separation and migration rates. To date, great efforts have been made to increase the charge separation efficiency, such as the loading of noble metals on the surface of the photocatalyst as cocatalysts,[7,8] or forming a composite photocatalyst between two kinds of semiconductors.[9–14] Another effective way to promote the charge separation rate is hybridizing a conjugated polymer with the semiconductor photocatalyst.[15–17]

Conjugated polymers such as polythiophenes, polypyrroles, polyanilines, poly(*p*-phenylenevinylene), and their derivates are extensively employed in photovoltaic devices as antenna layers for photovoltaic conversion of solar energy.[18–20] In recent years, conjugated polymers have also been widely applied in photocatalysis area to improve the photocatalytic properties of TiO_2. For example, Lin *et al.* synthesized polyaniline (PANI)/TiO_2 composite and found that its photocatalytic activity in degradation of methyl orange dye and 4-chlorine phenol was much higher than that of pure TiO_2.[21] Chu *et al.* reported that the photocatalytic properties of the TiO_2 were enhanced from the UV to the visible after incorporation of poly(3-hexylthiophene) (P3HT).[22] Yi *et al.* have prepared polythiophene (PT)/TiO_2 composite and investigated its photocatalytic performance in the degradation of methyl orange (MeO).[23] These studies demonstrate that the introduction of a conjugated polymer is an effective way to enhance the photocatalytic activity.

Among the conjugated polymers, poly(3-hexylthiophene) (P3HT) has attracted much attention due to its high charge carrier mobility, dissolubility and processability, long-term stability and broad absorption in visible region.[24] Especially, due to its extended π-conjugated system, it's considered to be an excellent hole transporter. Taking account of the efficient hole transporting ability of P3HT, we intended to design a composite photocatalyst by combining P3HT with an inorganic semiconductor, Bi_2WO_6, whose main oxidative species are holes.[25,26] It is expected that P3HT as an excellent hole conductor can transport the photo-generated holes to the surface of the semiconductor quickly to participate in the oxidation of pollutants, which can lead to an enhanced photocatalytic activity.

In this study, a novel P3HT/Bi_2WO_6 composite with high charge separation and migration efficiency was designed. The

School of Materials Science and Engineering, Shanghai Institute of Technology, 100 Haiquan Road, Shanghai, 201418, P.R. China. E-mail: xujiayue@sit.edu.cn; zjzhang@sit.edu.cn; Fax: +86-21-6087-3439; Tel: +86-21-6087-3581

P3HT/Bi_2WO_6 composite has a much higher hall mobility than bare Bi_2WO_6, suggesting the high charge transfer ability of the P3HT/Bi_2WO_6 composite. The photocatalytic activity evaluation, *via* the photo-degradation of a model pollutant, rhodamine B (RhB) under simulated solar light irradiation, demonstrated that the P3HT/Bi_2WO_6 composite showed much higher photocatalytic activity than bare Bi_2WO_6. Moreover, the mechanism of the enhanced photocatalytic activity was discussed in detail.

2. Experimental

2.1 Sample preparation

The reactants used in the experiment were analytical grade, without further purification. Bi_2WO_6 photocatalyst was synthesized *via* a hydrothermal method. In a typical process, 2 mmol of $Bi(NO_3)_3 \cdot 5H_2O$ was dissolved in 2 M nitric acid solution to obtain a transparent solution A. Meanwhile, 1 mmol of $Na_2WO_4 \cdot 2H_2O$ was dissolved in 30 mL of deionized water to get a transparent solution B. After that, solution A and solution B were mixed together to obtain a white suspension. NaOH solution was then added into the suspension until the pH value of the last suspension was about 1–2. After being stirred for several hours, the suspension was added to a 50 mL Teflon-lined autoclave up to 80% of the total volume. The autoclave was sealed in a stainless steel tank and heated at 160 °C for 20 h. Next, the autoclave was cooled to room temperature naturally. The final products were washed with deionized water for several times, and finally dried at 60 °C in air for 12 h.

P3HT/Bi_2WO_6 composites were prepared as follows: 0.3 g of the Bi_2WO_6 powder was added into 10 mL of CH_3Cl and dispersed under ultrasonic vibration for 30 min. Meanwhile, desired amount of P3HT was dissolved into 20 mL of CH_3Cl under magnetic stirring. Subsequently, the two solutions were mixed and stirred for 24 h at room temperature. Then the solvent was evaporated slowly in the vacuum and the obtained powders were dried in an oven at 60 °C for 12 h. The loading amount of P3HT was 0.25 wt%, 0.5 wt%, 0.75 wt% and 1 wt%, respectively.

2.2 Characterization

The phase and composition of the as-prepared samples were measured by X-ray diffraction (XRD) studies using an X-ray diffractometer with Cu Kα radiation under 40 kV and 20 mA and with the 2θ ranging from 20° to 70° (Rigaku, Japan). The morphologies and microstructures of the as-prepared samples were investigated by transmission electron microscopy (TEM, FEI Tecnai). FT-IR spectra of the samples were measured on a Nicolet iN10 (Thermo Fisher Scientific) FT-IR spectrometer. The KBr pellets were prepared with dried samples and the spectrum was collected in the range from 4000 to 400 cm^{-1}. UV-vis diffuse reflectance spectra (DRS) of the samples were recorded with a UV-vis spectrophotometer (Cary Series UV-Vis-NIR Spectrophotometer 5000) using $BaSO_4$ as a reference. The Hall mobility of the samples were measured on a Lake Shore 775 HMS Matrix by pressing the powders into a pellet. Photoelectrochemical measurements were performed in a three electrode quartz cells with 0.1 M Na_2SO_4 electrolyte solution. Saturated calomel electrode (SCE) and platinum wire were used as reference and counter electrodes, respectively. Bi_2WO_6 and P3HT/Bi_2WO_6 film electrodes on ITO served as the working electrode. The photoelectrochemical experiment results were recorded with an electrochemical system (CHI-650E, China) using a 500 W Xe lamp as the light source.

2.3 Photocatalytic test

Photocatalytic activities of the P3HT/Bi_2WO_6 composites and Bi_2WO_6 were evaluated by photocatalytic degradation of rhodamine B (RhB) under simulated solar light irradiation. A 500 W Xe lamp with the wavelength of $\lambda > 290$ nm was used as the light source. The experiments were conducted at room temperature as follows: 0.1 g of photocatalyst was added to 100 mL of RhB (10^{-5} mol L^{-1}) solution. Prior to irradiation, the suspensions were magnetically stirred for an hour in the dark to ensure the adsorption–desorption equilibrium between RhB and photocatalyst powders. At fixed time intervals, 3 mL suspension was sampled and centrifuged to remove the catalyst powders. After that, the supernatant was taken out to measure the absorption spectral change of RhB through a UV-vis spectrophotometer (Cary Series UV-Vis-NIR Spectrophotometer 5000) to monitor the photo-degradation rate. The concentration change of RhB was determined by monitoring the optical intensity of absorption spectra at 552 nm.

3. Results and discussion

3.1 Crystal structure

The phase structures of the prepared products were investigated by a powder X-ray diffractometer. The diffraction pattern in Fig. 1 shows that all the peaks can be indexed to the orthorhombic phase of Bi_2WO_6 according to the JCPDS card no. 39-0256 and no other crystalline phase can be detected. Compared with the XRD pattern of bare Bi_2WO_6, no distinct difference was observed on the P3HT/Bi_2WO_6 composites due to the low quality ratio of P3HT. This result implies that the crystalline

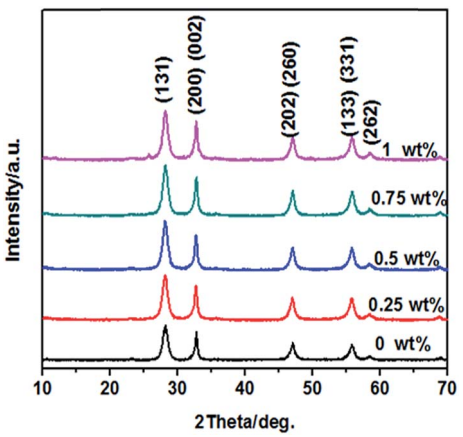

Fig. 1 XRD patterns of the as-prepared products.

phase of Bi_2WO_6 has not been changed by the modification of P3HT.

3.2 Morphology

The morphologies and microstructures of P3HT, Bi_2WO_6 and the P3HT/Bi_2WO_6 composite (0.5 wt%) were revealed by TEM, as shown in Fig. 2. As shown in Fig. 2(a), P3HT exhibits a porous spongy morphology. Both Bi_2WO_6 and the P3HT/Bi_2WO_6 composite display a two-dimensional plate-like morphology with lateral sizes of 100–200 nm, as shown in the panoramic view in Fig. 2(b) and (c). However, closer observation of the P3HT/Bi_2WO_6 composite in Fig. 2(d) and (e) shows that some tiny nanocrystals with sizes of 5–10 nm are decorated on the nanoplates, which could be ascribed to the existence of P3HT. Moreover, the high-resolution transmission electron microscopy (HRTEM) in Fig. 2(f) shows clear lattice spacing of the nanosheet matrix, which is consistent with the *d*-spacing (0.315 nm) of the (131) reflection of Bi_2WO_6.

3.3 FT-IR spectra analysis

Molecular structures of the resulting samples were characterized by FT-IR spectra in the range from 4000 to 400 cm^{-1}, as shown in Fig. 3. The characteristic peaks of P3HT and Bi_2WO_6 can be found in the spectra of the P3HT/Bi_2WO_6 composite. The main characteristic peaks of P3HT appear in the spectrum of P3HT/Bi_2WO_6 composite as follows: the peak at 2926 cm^{-1} is ascribed to the C–H stretching mode of the thiophene rings. The peak at 2854 cm^{-1} is attributed to the hexyl C–H stretching absorption, while the absorption peak at 1459 is assigned to the C=C stretching vibration on the thiophene ring.[27] Besides the characteristic peaks of P3HT, main absorption bands at 400–1000 cm^{-1}, which are attributed to Bi–O, W–O stretching, and W–O–W bridging stretching modes are also observed,[28] which indicates that the composite is composed of P3HT and Bi_2WO_6.

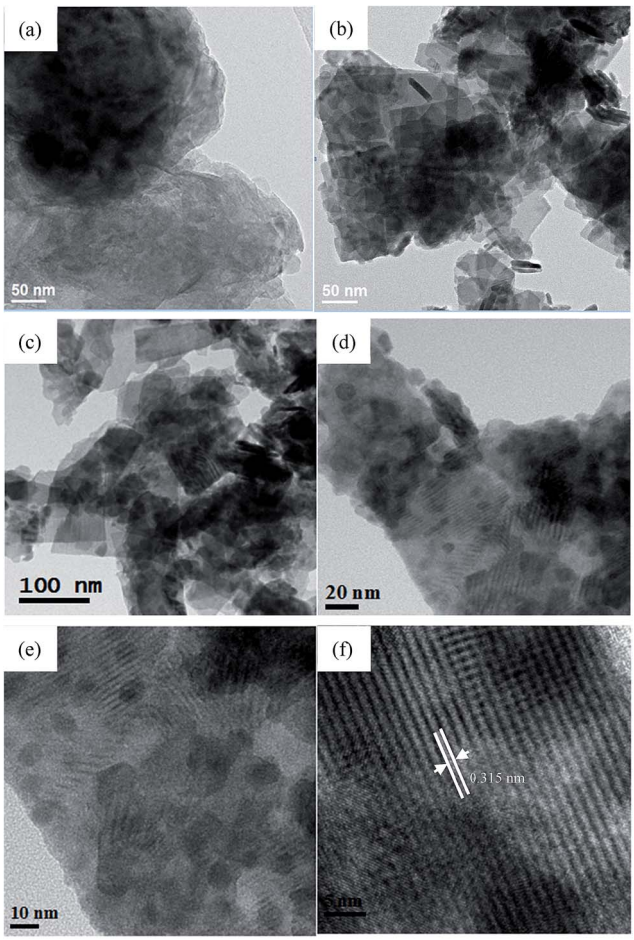

Fig. 2 (a) TEM image of P3HT; (b) TEM image of Bi_2WO_6; (c) and (d) TEM images of the P3HT/Bi_2WO_6 composite (0.5 wt%); (e) and (f) high resolution TEM images of the P3HT/Bi_2WO_6 composite (0.5 wt%).

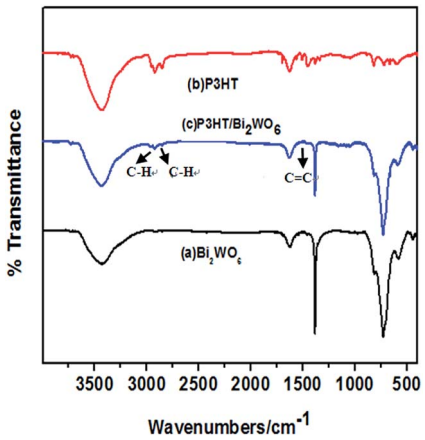

Fig. 3 FT-IR spectra of P3HT, Bi_2WO_6 and P3HT/Bi_2WO_6 composite (0.5 wt%).

3.4 UV-vis spectra

The UV-vis diffuse reflectance spectra (DRS) of the P3HT/Bi_2WO_6 composites are compared with that of bare Bi_2WO_6, as shown in Fig. 4. According to the spectra, bare Bi_2WO_6 sample shows the characteristic spectrum with its fundamental absorption edge at *ca.* 450 nm, corresponding to the band gap of 2.75 eV. It could be observed that with the introduction of P3HT, the absorption intensity of the P3HT/Bi_2WO_6 composites increases remarkably, which is attributed to the electron

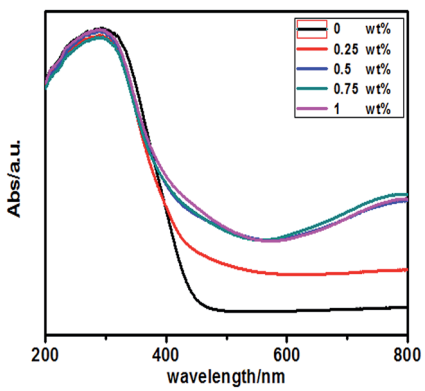

Fig. 4 UV-vis diffuse reflectance spectra of the as-prepared samples.

transition from the valence bond to the antibonding polaron state (π–π^* type) of P3HT.[29] Therefore, the P3HT/Bi_2WO_6 composite can harvest visible light effectively to generate more photo-induced electrons and holes, which could result in higher visible light photocatalytic activities.

3.5 Photocatalytic activity

In order to investigate the photocatalytic activity of the P3HT/Bi_2WO_6 composites, photo-degradation of RhB was carried out under simulated solar light irradiation. The photo-degradation efficiencies of RhB as a function of irradiation time in the presence of P3HT/Bi_2WO_6 composites compared to bare Bi_2WO_6 is shown in Fig. 5. Blank test (RhB solution without any photocatalyst) shows that RhB exhibits little photolysis, which demonstrates that RhB is quite stable under simulated solar light. Obviously, the introduction of P3HT into Bi_2WO_6 could significantly enhance the photocatalytic activity of the composite. When the loading amount of P3HT is 0.5 wt%, the sample shows the best photocatalytic performance, which could degrade RhB completely within 5 min. When the loading amount of P3HT further increases to 0.75 wt% and 0.1 wt%, the photocatalytic activities of the composites decrease as compared to that of 0.5 wt%, but still higher than that of bare Bi_2WO_6, which suggests that there is an optimum loading content for P3HT. It is estimated that when the loading amount of P3HT increases, more active reaction sites on the surface of Bi_2WO_6 are covered, and the photocatalytic activities decrease. Therefore, appropriate amount of P3HT could enhance the photocatalytic activity of Bi_2WO_6 effectively.

The stability of the photocatalyst is a main factor determining the potential for its practical application. In order to check the stability of the P3HT/Bi_2WO_6 composite, the photocatalyst was recycled and characterized by TEM and FT-IR spectra. As shown in Fig. 6(a), the morphology of the recycled P3HT/Bi_2WO_6 composite does not show obvious change, with the P3HT nanoparticles decorated on the Bi_2WO_6 nanoplates. Moreover, the FT-IR spectrum of the recycled P3HT/Bi_2WO_6 composite shown in Fig. 6(b) indicates that the characteristic peaks corresponding to the C–H stretching mode of the

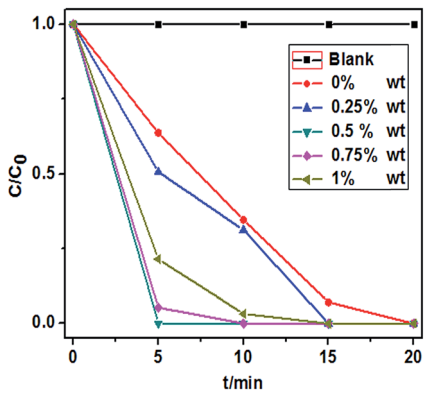

Fig. 5 Degradation efficiency of RhB as a function of time by the as-prepared samples under simulated solar light irradiation.

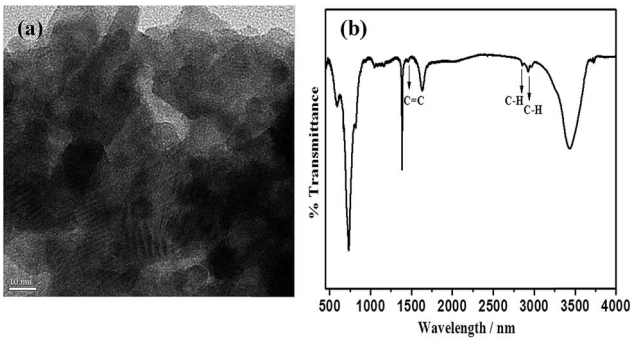

Fig. 6 TEM image (a) and FT-IR spectrum (b) of the recycled P3HT/Bi_2WO_6 composite.

thiophene rings, the hexyl C–H stretching absorption, and the C=C stretching vibration of P3HT molecule could be observed. These results demonstrate that the P3HT/Bi_2WO_6 composite is stable and is not photodegraded with time.

3.6 Mechanism of enhancement of photocatalytic activity

The photocatalytic process involves the generation of charge carriers such as electrons and holes induced by light, which then transfer to the surface of the semiconductor to participate in the oxidation of pollutants. Therefore, an ideal photocatalyst should have both a high charge separation efficiency and a high charge migration rate. The hybridization of P3HT could contribute to these two parameters in such two ways: first, P3HT is a p type semiconductor with a bandgap of 1.9–2.1 eV,[30] while Bi_2WO_6 is an n type semiconductor with a bandgap of *ca.* 2.8 eV.[31] Therefore, when Bi_2WO_6 is hybridized by P3HT, a p–n heterojunction would be formed and the charge carriers would diffuse in the opposite direction to form an internal electric field in the direction from n-type Bi_2WO_6 to p-type P3HT at the heterojunction interface. Under simulated solar light irradiation, the P3HT polymer absorbs photons and promotes an electron from the ground state into an excited state. The polymer π-orbital becomes the highest occupied molecular orbital (HOMO) and the π^*-orbital becomes the lowest unoccupied molecular orbital (LUMO). Simultaneously, electrons can be excited to the conduction band (CB) and leave holes in the valence band (VB) of Bi_2WO_6. Since the LUMO level of P3HT is more negative than the conduction band edge of Bi_2WO_6,[30,32] the photo-induced electrons of P3HT could transfer easily to Bi_2WO_6 *via* the well developed interface, while the photo-generated holes are effectively collected in the π-orbital of P3HT, as shown in Fig. 7. Due to the formation of the internal electric field, the migration of photo-generated carriers is promoted. In this way, the photo-induced charge carriers are separated effectively, resulting in higher photocatalytic activity.

Photocurrent is an effective method to reflect the generation, separation and migration efficiency of photogenerated charge carriers. Fig. 8 shows the photocurrent of Bi_2WO_6 and P3HT/Bi_2WO_6 samples under simulated solar light. It can be seen that the photocurrent generated from P3HT/Bi_2WO_6 composite is larger than that of pure Bi_2WO_6. The increased photocurrent

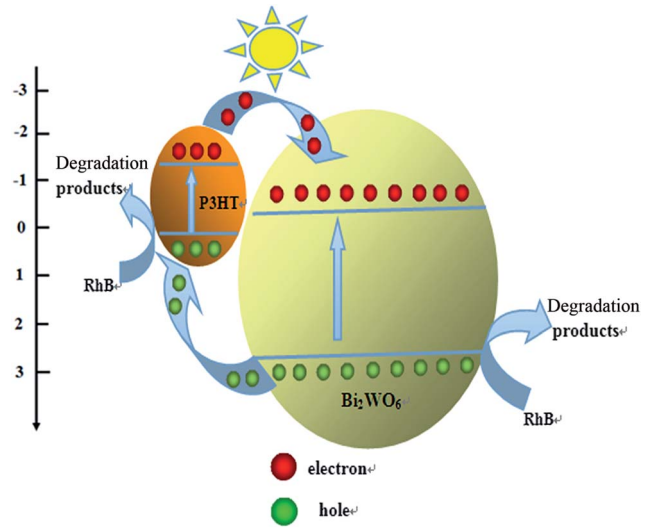

Fig. 7 Schematic representation of interfacial charge separation in P3HT/Bi_2WO_6 composite.

could be attributed to the higher separation efficiency of photogenerated electron–hole pairs, which is beneficial to the enhancement of photocatalytic activity.

More importantly, due to its special conjugated structure, P3HT is an excellent hole conductor, and the photo-generated holes can be transported easily through the π-conjugated bond of P3HT. Coincidently, the main oxidative species in the Bi_2WO_6 photocatalysis system are holes. To further confirm this, the trapping experiments of radicals were performed using *tert*-butyl alcohol (*t*BuOH) as a hydroxyl radical scavenger, and EDTA-2Na as a hole radical scavenger, respectively.[33,34] As shown in Fig. 9, the photocatalytic activity of P3HT/Bi_2WO_6 is hardly inhibited by adding free radical scavenger, while the photocatalytic activity of P3HT/Bi_2WO_6 is severely suppressed by the addition of hole scavenger. This indicates that the photo-generated holes are the major oxidative species in the P3HT/Bi_2WO_6 system on the degradation of RhB. The high hole carrier mobility of P3HT can enable the photo-generated holes to migrate to composite/solution interface easily to participate in the oxidation reaction, which is beneficial to the enhancement

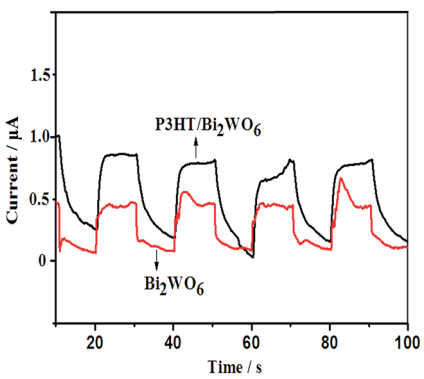

Fig. 8 Photocurrent response for Bi_2WO_6 and P3HT/Bi_2WO_6 composite.

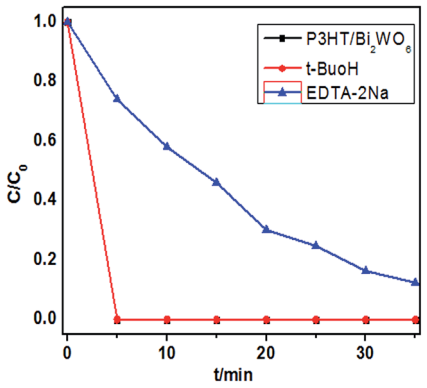

Fig. 9 Photocatalytic degradation of RhB by P3HT/Bi_2WO_6 composite photocatalyst with different scavengers under simulated solar light irradiation.

of the photocatalytic activity. In order to compare the charge transfer ability of Bi_2WO_6 and P3HT/Bi_2WO_6, the hall mobility of the two samples were tested. The result shows that the hall mobility of test samples of Bi_2WO_6 and P3HT/Bi_2WO_6 (0.5 wt%) are 3.0159×10^2 cm^2 V^{-1} s^{-1} and 4.7197×10^2 cm^2 V^{-1} s^{-1}, respectively, which indicates that hybridizing P3HT can improve the charge transfer rate of Bi_2WO_6 effectively. Therefore, due to the high charge separation and transportation efficiency, the P3HT/Bi_2WO_6 composite exhibits excellent photocatalytic performance.

4. Conclusion

In summary, a novel P3HT/Bi_2WO_6 composite photocatalyst with high charge separation and transportation efficiency was synthesized. The composite photocatalyst exhibited excellent photocatalytic activity in degradation of RhB under simulated solar light irradiation, which was much higher than that of bare Bi_2WO_6. The enhanced activity can be attributed to the effective separation of electron–holes pairs due to the formation of the internal electric field between P3HT and Bi_2WO_6, as well as the high hole carrier mobility of P3HT, which can transport the photo-generated holes to composite/solution interface quickly to participate in the oxidation of pollutants. Such a composite photocatalyst is promising for water purification and environmental remediation.

Acknowledgements

This work was supported by the National Natural Science Foundation of China (51402194), the Shanghai Science and Technology Committee (14YF1410700), the Shanghai Education Commission (15ZZ097), and the Program for Professor of Special Appointment (Eastern Scholar) at Shanghai Institutions of Higher Learning (4521ZK120053002).

References

1 A. Hagfeldt and M. Gratzel, *Chem. Rev.*, 1995, **95**, 49–68.

2 A. Kubacka, M. Fernández-García and G. Colón, *Chem. Rev.*, 2012, **112**, 1555–1614.
3 J. S. Zhang, M. W. Zhang, R. Q. Sun and X. C. Wang, *Angew. Chem.*, 2012, **124**, 10292–10296.
4 M. R. Hoffmann, S. T. Martin, W. Choi and D. W. Bahnemann, *Chem. Rev.*, 1995, **95**, 69–96.
5 K. Maeda and K. Domen, *J. Phys. Chem. Lett.*, 2010, **1**, 2655–2661.
6 M. Schwab, M. Hamburger, X. Feng, J. Shu, H. Spiess, X. Wang, M. Antonietti and K. Mullen, *Chem. Commun.*, 2010, **46**, 8932–8934.
7 H. Yan, J. Yang, G. Ma, G. Wu, X. Zong, Z. Lei, J. Shi and C. Li, *J. Catal.*, 2009, **266**, 165–168.
8 K. Maeda, A. Xiong, T. Yoshinaga, T. Ikeda, N. Sakamoto, T. Hisatomi, M. Takashima, D. Lu, M. Kanehara, T. Setoyama, T. Teranishi and K. Domen, *Angew. Chem., Int. Ed.*, 2010, **49**, 4190–4193.
9 Y. F. Liu, W. Q. Yao, D. Liu, R. L. Zong, M. Zhang, X. G. Ma and Y. F. Zhu, *Appl. Catal., B*, 2015, **163**, 547–553.
10 Y. Liu, F. Xin, F. Wang, S. Luo and X. Yin, *J. Alloys Compd.*, 2010, **498**, 179–184.
11 D. Yue, D. M. Chen, Z. H. Wang, H. Ding, R. L. Zong and Y. F. Zhu, *Phys. Chem. Chem. Phys.*, 2014, **16**, 26314–26321.
12 W. H. He, R. R. Wang, L. Zhang, J. Zhu, X. Xiang and F. Li, *J. Mater. Chem. A*, 2015, **3**, 17977–17982.
13 X. Xiang, L. S. Xie, Z. W. Li and F. Li, *Chem. Eng. J.*, 2013, **221**, 222–229.
14 W. H. He, Y. Yang, L. R. Wang, J. J. Yang, X. Xiang, D. P. Yan and F. Li, *ChemSusChem*, 2015, **8**, 1568–1576.
15 H. J. Yan and Y. Huang, *Chem. Commun.*, 2011, **47**, 4168–4170.
16 Y. W. Su, W. H. Lin, Y. J. Hsu and K. H. Wei, *Small*, 2014, **10**, 4427–4442.
17 K. R. Reddy, M. Hassan and V. G. Gomes, *Appl. Catal., A*, 2015, **489**, 1–16.
18 I. Gonzalez-Valls and M. Lira-Cantu, *Energy Environ. Sci.*, 2009, **2**, 19–34.
19 B. Kippelen and J. Bredas, *Energy Environ. Sci.*, 2009, **2**, 251–261.
20 M. Helgesen, R. Søndergaard and F. C. Krebs, *J. Mater. Chem.*, 2010, **20**, 36–60.
21 Y. M. Lin, D. Z. Li, J. H. Hu, G. C. Xiao, J. X. Wang, W. J. Li and X. Z. Fu, *J. Phys. Chem. C*, 2012, **116**, 5764–5772.
22 J. H. Huang, M. A. Ibrahem and C. W. Chu, *RSC Adv.*, 2013, **3**, 26438–26442.
23 Y. Zhu, S. Xu and D. Yi, *React. Funct. Polym.*, 2010, **70**, 282–287.
24 D. E. Motaung, G. F. Malgas, C. J. Arendse, S. E. Mavundla, C. J. Oliphant and D. Knoesen, *Sol. Energy Mater. Sol. Cells*, 2009, **93**, 1674–1680.
25 H. B. Fu, C. S. Pan, W. Q. Yao and Y. F. Zhu, *J. Phys. Chem. B*, 2005, **109**, 22432–22439.
26 Y. J. Wang, X. J. Bai, C. S. Pan, J. He and Y. F. Zhu, *J. Mater. Chem.*, 2012, **22**, 11568–11573.
27 D. S. Wang, J. Zhang, Q. Z. Luo, X. Y. Li, Y. D. Duan and J. An, *J. Hazard. Mater.*, 2009, **169**, 546–550.
28 Z. J. Zhang, W. Z. Wang and E. P. Gao, *J. Mater. Sci.*, 2014, **49**, 7325–7332.
29 Y. F. Zhu and Y. Dan, *Sol. Energy Mater. Sol. Cells*, 2010, **94**, 1658–1664.
30 X. J. Bai, C. P. Sun, S. L. Wu and Y. F. Zhu, *J. Mater. Chem. A*, 2015, **3**, 2741–2747.
31 Q. Xiao, J. Zhang, C. Xiao and X. K. Tan, *Catal. Commun.*, 2008, **9**, 1247–1253.
32 Z. J. Zhang, W. Z. Wang, L. Wang and S. M. Sun, *ACS Appl. Mater. Interfaces*, 2012, **4**, 593–597.
33 M. Zhang, W. Q. Yao, Y. H. Lv, X. J. Bai, Y. F. Liu, W. J. Jiang and Y. F. Zhu, *J. Mater. Chem. A*, 2014, **2**, 11432–11438.
34 Y. Y. Zhu, Y. F. Liu, Y. H. Lv, Q. Ling, D. Liu and Y. F. Zhu, *J. Mater. Chem. A*, 2014, **2**, 13041–13048.